

Modeling benzene orientational randomization in Na–Y zeolite at finite loadings with kinetic Monte Carlo and master equation methods

Cristian Blanco, Chandra Saravanan,^{a)} and Melissa Allen

Department of Chemistry, University of Massachusetts, Amherst, Massachusetts 01003

Scott M. Auerbach^{b)}

Department of Chemistry and Department of Chemical Engineering, University of Massachusetts, Amherst, Massachusetts 01003

(Received 30 June 2000; accepted 6 September 2000)

We have modeled the orientational dynamics of benzene in Na–Y zeolite, motivated by the NMR study of Isfort *et al.* at loadings of five benzenes per cage [Chem. Phys. Lett. **288**, 71 (1998)]. We consider guest-guest interactions in two stages: first, we include only site blocking; next, we consider both site blocking and nearest-neighbor attractions. We calculated orientational correlation functions using kinetic Monte Carlo and also with a mean field master equation (MFME). Both methods produce correlation functions exhibiting biexponential decay in time. Analytically solving the MFME shows that long-time decay is controlled by a composite of intracage and cage-to-cage jumps. The apparent activation energy is *greater* than the fundamental cage-to-cage barrier when considering only site blocking, but is *less* than the same fundamental barrier when also including guest-guest attractions. This suggests that the actual cage-to-cage barrier is greater than the 40 kJ mol⁻¹ reported by Isfort *et al.*, which lends credence to previous simulations of benzene in Na–Y.

© 2000 American Institute of Physics. [S0021-9606(00)70145-0]

I. INTRODUCTION

The transport properties of adsorbed molecules play a central role in separations and reactions that take place within zeolites and other nanoporous solids.^{1,2} Significant effort has been devoted to understanding intracrystalline self diffusion in zeolites using pulsed field gradient nuclear magnetic resonance (NMR),¹ which directly probes adsorbate center-of-mass translational motion along a magnetic field gradient. Modeling such transport processes can help reveal the mechanisms of intracrystalline diffusion.^{3–5} Complementary to translational motion is orientational dynamics, which provides information that may be obfuscated by or even invisible to diffusion measurements.⁶ Orientational dynamics in zeolites has been probed by NMR relaxation,^{7–9} exchange-induced sidebands (EIS) NMR,^{10,11} and multidimensional exchange NMR.^{12,13} In this article, we develop and apply kinetic modeling techniques to study the orientational randomization of benzene in Na–Y zeolite at finite loadings, to reveal how the competition between host-guest adhesion and guest-guest cohesion controls orientational dynamics in zeolites.

Auerbach and Metiu reported kinetic Monte Carlo (KMC) simulations of benzene dynamics at infinite dilution in Na–Y, with different numbers of supercage cations corresponding to various Si:Al ratios.⁶ We found that full cation occupancy gives randomization rates controlled by intracage motion,⁸ whereas half cation occupancy gives rates sensitive to *both* intracage and intercage motion. This finding

prompted Favre *et al.* to perform EIS NMR experiments on benzene in Ca–Y with half cation occupancy (Si:Al=2.0), finding indeed that they were able to measure both the intracage and cage-to-cage jump rates within a single experiment.¹¹ Isfort *et al.* reported a two-dimensional exchange NMR study on benzene in Na–Y with full cation occupancy at high benzene loadings (5.1 molecules per supercage),¹³ finding an apparent activation energy controlling orientational randomization of 40±2 kJ mol⁻¹. Although it is tempting to compare this energy favorably with previously simulated intercage barriers for benzene in Na–Y, ranging from 41 to 49 kJ mol⁻¹,^{14–16} we know that benzene orientational randomization in such a material is often controlled by intracage dynamics rather than by cage-to-cage migration. Moreover, it is not obvious how loading effects will alter the balance between different pathways of orientational randomization. In this article, we address these issues by computing orientational correlation functions for benzene in Na–Y at finite loadings using KMC simulations and mean field approximations.

We consider guest-guest interactions in two stages: first, we include only site blocking; next, we consider both site blocking and nearest-neighbor attractions with our previously reported parabolic jump model.^{17,18} We find that orientational correlation functions generally exhibit biexponential decay at finite loadings, with a long-time decay rate that depends sensitively on the treatment of guest-guest interactions. In the end, we predict that the actual cage-to-cage barrier is slightly greater than the 40±2 kJ mol⁻¹ reported by Isfort *et al.*, which lends credence to the previous simulations of benzene in Na–Y.

The remainder of this article is organized as follows: in Sec. II we present our general model of benzene orientational

^{a)}Present address: Department of Chemistry, UC Berkeley, Berkeley, CA 94720.

^{b)}Author to whom correspondence should be addressed. Electronic mail: auerbach@chem.umass.edu

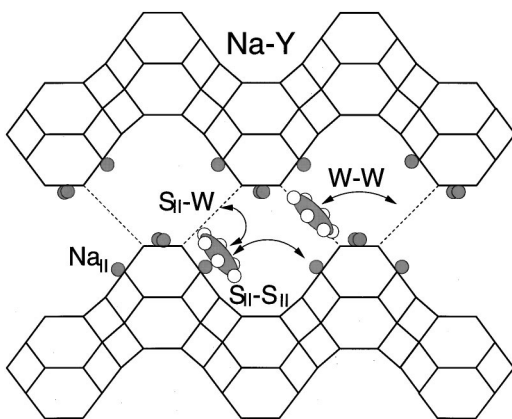


FIG. 1. Sorption sites and jumps for benzene in Na–Y.

randomization in Na–Y at finite loadings. In Sec. III we review the KMC simulation methodology, and describe the mean field approaches used for comparison with the KMC results. In Sec. IV we present our theory and simulation results in the context of the experimental data discussed above, and in Sec. V we offer concluding remarks.

II. GENERAL MODEL

We model benzene orientational randomization in Na–Y by replacing the zeolite framework with a three dimensional lattice of binding sites. Such a lattice model reproduces dynamical behavior accurately when site residence times are much longer than travel times between sites,^{12,19} which is the case for benzene in Na–Y because of the strong charge-quadrupole interaction between Na⁺ and benzene. Benzene has two predominant sites at infinite dilution in Na–Y.²⁰ In the primary site, denoted as S_{II}, benzene is facially coordinated to a supercage six-ring, ca. 2.7 Å above Na(II). In the secondary site, denoted as W, benzene lies in the plane of the 12-ring window separating adjacent supercages, ca. 5.3 Å from the S_{II} site. The lattice of benzene binding sites in Na–Y contains four tetrahedrally arranged S_{II} sites and four tetrahedrally arranged, doubly shared W sites per supercage, as shown in Fig. 1.

This lattice model was derived in previous work¹⁴ by assuming a Si:Al ratio of 2.0, hence zeolite Y, which requires 64 Na ions per unit cell to balance charge. We assume full occupation of Na sites I' (32 per unit cell, located in smaller β cages) and II (32 per unit cell, located in supercages). This occupancy model is reasonable considering that only the Na(II) ions are accessible to a penetrant the size of benzene. In addition, diffraction studies of Na–Y (Si:Al = 1.7) find nearly full Na(II) occupation.²⁰

Benzene orientational dynamics at finite loadings involve jump angles and site-to-site rate constants modified by guest-guest interactions. Repulsive guest-guest interactions, which typically act over very short length scales, can be treated simply by excluding multiple occupancy of sites, i.e., the site-blocking or Langmuirian model.²¹ This model assumes that the loading dependence of adsorption and transport is controlled largely by excluded-volume entropic effects. Repulsive interactions can also change the nature and

TABLE I. Activation energies and Arrhenius prefactors for benzene in Na–Y.

Jump	Activation energy (eV)	Arrhenius prefactor (s ⁻¹)
S _{II} →S _{II}	0.25	0.8×10 ¹³
S _{II} →W	0.38	0.8×10 ¹³
W→S _{II}	0.13	1.1×10 ¹²
W→W	0.13	2.4×10 ¹¹

distribution of adsorption sites at high loadings, as is predicted, e.g., for Xe in Na–A.²² The large-pore nature of Na–Y cages, and the molecular recognition of benzene by 12-ring windows, makes this latter effect much less important for benzene in Na–Y.

Attractive interactions between neutral guests, which typically act over medium but not long length scales, can influence the energetics of adsorption and transport for finite loadings. In particular, benzene site-to-site jump angles can be modified from their near-tetrahedral values at infinite dilution because quadrupole-quadrupole interactions make benzene-benzene ‘‘T-shaped’’ configurations more favorable.⁶ On average, we expect these deviations from tetrahedral jump angles to be relatively small because of the strong host-guest forces. To complicate matters further, small jump angles have been observed experimentally for benzene at finite loadings in Na–Y,¹³ because of spectator benzenes that adjust to the local effect of a nearby site-to-site jump. These are very difficult to account for in a lattice model, and hence will be ignored in the present study. As such, our model consists simply in terms of tetrahedral site-to-site jump angles. Saturation coverages of five to six molecules per cage are found for benzene in Na–Y,^{13,23} which roughly corresponds to occupation of all S_{II} and W sites.

Guest-guest interactions can also modify jump activation energies of site-to-site rate coefficients, depending upon specific configurations of neighboring benzenes. In order to account for this effect when modeling diffusion in zeolites,¹⁸ we have generalized an approach used previously by Hood *et al.*²⁴ that relates binding energies to transition state energies. In this method, we assume that the minimum energy hopping path connecting adjacent sorption sites is characterized by intersecting parabolas; details can be found in Ref. 18. We adopt this approach for modeling molecular orientational dynamics in zeolites at finite loadings. In what follows, the W and S_{II} sites are labeled sites 1 and 2, respectively.

A lattice gas model is used to describe the system, limiting the range of adsorbate-adsorbate interactions to nearest neighbors, as introduced by Saravanan and Auerbach in a previous paper.¹⁸ The infinite dilution site-to-site jump activation energies and Arrhenius prefactors, calculated from transition state theory with dynamical corrections for benzene in Na–Y,¹⁵ are given in Table I. These are used to determine the infinite dilution jump rates assuming the Arrhenius temperature dependence $k_{ij} = \nu_{ij} e^{-BE_a(i,j)}$, where $\beta = 1/k_B T$. The lattice gas coupling parameters, J_{ij} , are obtained from the second virial coefficient of the heat of

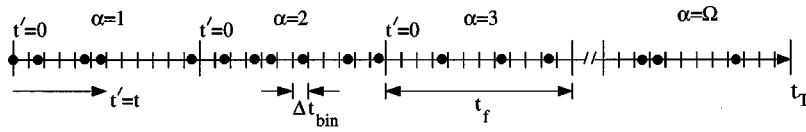


FIG. 2. Schematic of KMC run of total duration t_T split into Ω trajectories of duration t_f , showing the division of each trajectory into time bins of width Δt_{bin} . The dark circles indicate time instances when jump events takes place.

adsorption,^{25,26} yielding ca. $J = J_{22} \cong J_{21} = -0.04$ eV. J_{11} is set to zero because the W-W intracage distance is larger than typical $S_{\text{II}}-S_{\text{II}}$ and W- S_{II} intracage distances [$d(S_{\text{II}}, S_{\text{II}}) \approx d(S_{\text{II}}, \text{W}) \approx 5$ Å, and $d(\text{W}, \text{W}) \approx 9$ Å].²⁰

III. METHODOLOGY

In this section we describe three methods of determining orientational correlation functions (OCFs) at finite loadings. In Sec. III A, we describe kinetic Monte Carlo (KMC) simulations for calculating OCFs; in Sec. III B we describe a mean field matrix equation approach for determining OCFs numerically and analytically; and in Sec. III C we describe a mean field theory that describes short-time behavior of the OCF.

A. KMC simulations

We apply both fixed and variable time-step KMC methods for calculating OCFs. This is because variable time-step methods are efficient for sampling jumps with widely varying time scales, while fixed time-step methods are convenient for calculating ensemble averaged correlation functions. We perform an ensemble average by computing a single, long KMC random walk with variable time steps, which is divided into an ensemble of Ω trajectories each with duration t_f , as shown in Fig. 2. The initial configuration of trajectory $\alpha+1$ is obtained from the final configuration of the α th trajectory. Each initial condition occurs with the proper Boltzmann probability because canonical KMC obeys detailed balance. The time scale t_f is the longest time for which we can compute the OCF; as such t_f must be adjusted to encompass the dynamics we wish to study.

Our simulations are performed on either $1^3=1$ or $2^3=8$ FAU unit cells with periodic boundary conditions. Each unit cell contains $M=48\mathcal{N}$ sites consisting of $M_1=16\mathcal{N}$ W sites and $M_2=32\mathcal{N}$ S_{II} sites, where \mathcal{N} is the number of unit cells in the simulation. For a given configuration, \vec{n} , of random walkers, a process list of possible hops from occupied to empty sites is compiled for all molecules. A particular jump from site i to j is chosen from this list with a probability of $k_{i \rightarrow j}/k_{\text{tot}}(\vec{n})$, where $k_{i \rightarrow j}$ is the i to j jump rate coefficient, and $k_{\text{tot}}(\vec{n})$ is the sum of all rate coefficients in the process list. A hop is made every KMC step and the system clock is updated with variable time steps.²⁷ The time instances corresponding to these hop events are indicated using dark circles in Fig. 2. The actual KMC time step is obtained from $\Delta t(\vec{n}) = -\ln(1-x_1)/k_{\text{tot}}(\vec{n})$, where $x_1 \in [0,1)$ is a uniform random number.

The OCF for the i th molecule at time t , $C_i(t)$, is calculated according to

$$C_i(t) = \langle C_{\alpha,i}(t) \rangle = \frac{1}{\Omega} \sum_{\alpha=1}^{\Omega} C_{\alpha,i}(t) \\ = \frac{1}{\Omega} \sum_{\alpha=1}^{\Omega} P_2[\cos(\gamma_{\alpha,i}(t))], \quad (3.1)$$

where $P_2(x) = 1/2(3x^2 - 1)$ is the second order Legendre polynomial, and $\gamma_{\alpha,i}(t)$ is the angle between the molecule's sixfold axis at $t'=0$ and $t'=t$. To calculate this average, a constant time-step grid is superimposed on the KMC-calculated sequence of jump events, as shown in Fig. 2. The time bin width, Δt_{bin} , is usually chosen so that $t_f/\Delta t_{\text{bin}} \cong 10^2 - 10^3$, depending on the loading. For molecule i in trajectory α , we compute the normalized dot product between the molecule's sixfold axis at time 0 and $t = m\Delta t_{\text{bin}}$, i.e., $\cos[\gamma_{\alpha,i}(m)]$. The OCF for the molecule at $t = m\Delta t_{\text{bin}}$ is determined by averaging $P_2[\cos(\gamma_{\alpha,i}(m))]$ over all Ω trajectories. We note that this average can be accumulated simultaneously as the KMC random walk is performed, precluding the need to store system configurations at all times.

All the calculations are performed using a four node IBM 604e Power PC RS/6000 working at 333 MHz. The largest calculation, based on a fractional loading of $\theta=0.9$ at 200 K in a 2^3 cell, required 38 CPU hours.

B. Mean field master equation

We now describe a mean field master equation (MFME) approach for determining the OCF of benzene in Na-Y. Such an approach is useful for several reasons. First, the MFME energetics are exact for very low and very high loadings, and as such can be used to check the KMC results. Second, comparing MFME and KMC results for intermediate loadings can shed light on the extent to which orientational randomization can be described by mean field approximations. Third, solving the MFME is very rapid compared to performing KMC simulations, and as such may provide a more computationally efficient route to understanding benzene orientational randomization. Finally, symbolic algebra programs can be used to obtain analytical solutions of the MFME, which yield remarkably simple formulas and hence important insights in certain physical limits.

Given that a molecule is initially at site l , the conditional probability that the molecule is present in any site k at time $t > 0$, $p(k, t | l, 0)$, can be used to evaluate the OCF according to

$$\begin{aligned}
C(t) &= \langle P_2[\cos(\gamma)] \rangle \\
&= \sum_{l=1}^M \sum_{k=1}^M P_2[\cos(\gamma(k,l))] \cdot p(k,t|l,0) \cdot p_l \\
&= \frac{P_W}{M_1} \sum_{l=1}^{M_1} \sum_{k=1}^M P_2[\cos(\gamma(k,l))] \cdot p(k,t|l,0) \\
&\quad + \frac{P_{S_{II}}}{M_2} \sum_{l=M_1+1}^M \sum_{k=1}^M P_2[\cos(\gamma(k,l))] \cdot p(k,t|l,0),
\end{aligned} \tag{3.2}$$

where M_1 , M_2 and M are the number of W, S_{II} and total sites in the system, respectively. In Eq. (3.2), p_l is the equilibrium probability to occupy site number l , while P_W and $P_{S_{II}}$ are the equilibrium probabilities to occupy any S_{II} or W site, respectively. As such, $P_W = M_1 \cdot p_l$ for $l = 1, \dots, M_1$, and $P_{S_{II}} = M_2 \cdot p_l$ for $l = M_1 + 1, \dots, M$. In addition, $\gamma(k,l)$ is the orientation of the molecule's sixfold axis in site k relative to its initial position in site l . The probabilities $P_{S_{II}}$ and P_W are computed in Sec. III B 1, and the function $p(k,t|l,0)$ is evaluated by fixing the initial conditions and solving the MFME as discussed in Sec. III B 2.

1. Determining $P_{S_{II}}$ and P_W

We have previously described a mean field theory for determining equilibrium properties for this lattice model.^{17,18} For completeness, we briefly describe the method of evaluating the probabilities, $P_{S_{II}}$ and P_W .

In the Na–Y lattice, with twice as many S_{II} sites as W sites, P_W is given by $\theta_1 / (\theta_1 + 2\theta_2)$, where θ_1 and θ_2 are the fractional coverages on W and S_{II} sites, respectively. Since the probabilities of occupying the S_{II} and W sites are mutually exclusive, $P_{S_{II}} = 1 - P_W = 2\theta_2 / (\theta_1 + 2\theta_2)$. We approximate the loading dependence of $P_{S_{II}}$ and P_W from mean field theory in the grand canonical ensemble by averaging over local fluctuations in the instantaneous energy of each adsorption site. The occupancies in W and S_{II} sites are Boltzmann averaged to determine θ_1 and θ_2 ,²⁸ according to

$$\theta_1 \cong \frac{e^{-\beta(f_1 - \mu) + 6(J_{11}\theta_1 + J_{12}\theta_2)}}{1 + e^{-\beta(f_1 - \mu) + 6(J_{11}\theta_1 + J_{12}\theta_2)}}, \tag{3.3}$$

$$\theta_2 \cong \frac{e^{-\beta(f_2 - \mu) + 3(J_{22}\theta_2 + J_{12}\theta_1)}}{1 + e^{-\beta(f_2 - \mu) + 3(J_{22}\theta_2 + J_{12}\theta_1)}}, \tag{3.4}$$

where μ is the chemical potential and $f_i = \varepsilon_i - Ts_i$ are site free energies for S_{II} and W sites. We solve these simultaneous nonlinear equations for θ_1 and θ_2 self-consistently using the Newton–Raphson method.²⁹ In this study, as with our previous ones,^{14,18} the site binding energies are taken as $\varepsilon_2 = -0.78$ eV and $\varepsilon_1 = -0.53$ eV for benzene in Na–Y.³⁰ Site 2 is chosen for the zero of entropy in Na–Y, giving $s_2 \equiv 0$. Previous Monte Carlo simulations for benzene in Na–Y have yielded $s_1 = 1.98k_B = 0.00017$ eV/K.¹⁵

2. Determining $p(k,t|l,0)$

We now describe the MFME equation approach for obtaining the conditional probabilities $p(k,t|l,0)$ at finite loadings. Benzene in Na–Y can occupy $M_1 = 16\mathcal{N}$ W sites and $M_2 = 32\mathcal{N}$ S_{II} sites in the simulation cell. For the following discussion we remind the reader that the indices $l, k = 1, \dots, M_1$ denote W sites and $l, k = M_1 + 1, \dots, M$ denote S_{II} sites. On average all W sites are identical. Therefore, in order to evaluate $p(k,t|l,0)$ for the fraction of molecules beginning their trajectories at W sites, we choose the initial condition as $p(k,0|l=1,0) = \delta_{k,1}$ for all k . Using similar arguments, the initial condition for the fraction of molecules beginning their trajectories at S_{II} sites is chosen as $p(k,0|l = M_1 + 1, 0) = \delta_{k, M_1 + 1}$ for all k . The conditional probabilities are then determined by solving the following MFME:

$$\frac{dp_k(t)}{dt} = \sum_{j=1}^M W_{kj} p_j(t), \tag{3.5}$$

where $p_k(t)$ is the probability of a molecule to be in site k at time t , and W_{kj} is the total jump frequency of molecules from site j to a nearest-neighbor site k . The connectivity of sites in W_{kj} is consistent with applying periodic boundary conditions. The term W_{kk} represents the negative of the sum of rate coefficients for jumps that deplete the probability at site k , i.e., $W_{kk} = -\sum_{j=1, j \neq k}^M W_{kj}$. At finite loadings we apply a mean field approximation to these rate coefficients, i.e., W_{kj} is approximated by $W_{kj}^0(1 - \theta_1)$ if j is a W site, and by $W_{kj}^0(1 - \theta_2)$ if j is an S_{II} site. W_{kj}^0 are obtained from infinite dilution rate coefficients, and θ_1 and θ_2 are the equilibrium fractional site occupancies calculated using mean field theory discussed in Sec. III B 1. This approximation allows us to study the time dependence of the probabilities $p_k(t)$ by solving a system of *linear* differential equations. The more realistic self-consistent treatment would yield rather cumbersome nonlinear equations.

It is convenient for what follows to introduce a column vector $\mathbf{p}(t)$ and the transition matrix \mathbf{W} in order to rewrite Eq. (3.5) as

$$\frac{d\mathbf{p}(t)}{dt} = \mathbf{W}\mathbf{p}(t). \tag{3.6}$$

The solution of this master equation can be given using the eigenvalues and eigenvectors of a symmetric matrix, $\tilde{\mathbf{W}}$, which is given by the geometric mean of W_{kj} and its transpose element:³¹

$$\tilde{W}_{kj} = (W_{kj}W_{jk})^{1/2}. \tag{3.7}$$

Using the microscopic reversibility condition, $p_j(t_{eq}) \cdot W_{jk} = p_k(t_{eq}) \cdot W_{kj}$, where $p_k(t_{eq})$ and $p_j(t_{eq})$ are the equilibrium probabilities of occupying sites k and j , respectively, Eq. (3.7) can be rewritten as follows:

$$\tilde{W}_{kj} = W_{kj} \left[\frac{p_k(t_{eq})}{p_j(t_{eq})} \right]^{1/2}. \tag{3.8}$$

It is clear from Eqs. (3.7) and (3.8) that the diagonal terms remain unchanged in this transform, i.e., $\tilde{W}_{kk} = W_{kk}$. Given the eigenvectors and eigenvalues of \mathbf{W} , $\{\chi_i\}$ and $\{\lambda_i\}$, respectively, i.e.,

$$\mathbf{W}\chi_i = \lambda_i\chi_i \quad (i = 1, 2, \dots, M), \quad (3.9)$$

it can be shown that the matrix $\tilde{\mathbf{W}}$ has the same eigenvalues $\{\lambda_i\}$ as \mathbf{W} .³¹⁻³³ However, the eigenvectors of $\tilde{\mathbf{W}}$ are given by $\tilde{\chi}_i = \chi_i / [p_i(t_{\text{eq}})]^{1/2}$. Under the above transformations, Eq. (3.9) becomes

$$\tilde{\mathbf{W}}\tilde{\chi}_i = \lambda_i\tilde{\chi}_i, \quad (3.10)$$

where $\tilde{\mathbf{W}}$ is by construction a symmetric matrix. Hence all its eigenvalues, $\{\lambda_i\}$, are real and the corresponding eigenvectors, $\tilde{\chi}_i$, are orthonormal. This also shows that an eigenvector, $\{[p_1(t_{\text{eq}})]^{1/2}, [p_2(t_{\text{eq}})]^{1/2}, \dots, [p_M(t_{\text{eq}})]^{1/2}\}$, exists whose corresponding eigenvalue is zero.³¹⁻³³ This simply implies that the system of Eqs. (3.6) is linearly dependent because of the microscopic reversibility condition.

In what follows, we discuss the method of solving Eq. (3.6). The eigenvalues and eigenvectors of $\tilde{\mathbf{W}}$ are obtained by routine diagonalization. A matrix \mathbf{V} given by $\mathbf{V} = \{\chi_1, \chi_2, \dots, \chi_M\} = \{\tilde{\chi}_1 p_1(t_{\text{eq}})^{1/2}, \tilde{\chi}_2 p_2(t_{\text{eq}})^{1/2}, \dots, \tilde{\chi}_M p_M(t_{\text{eq}})^{1/2}\}$, consisting of the scaled eigenvectors of $\tilde{\mathbf{W}}$, is constructed. When there is no degeneracy in eigenvalues, the solution of Eq. (3.6) is given simply by

$$\mathbf{p}(t) = \mathbf{V} \text{diag}[e^{\lambda_j t}] \mathbf{V}^{-1} \mathbf{p}(0), \quad (3.11)$$

where $\mathbf{p}(0)$ corresponds to the initial state of the system.³⁴ However, when degenerate eigenvalues are present, the solution is given using the matrix \mathbf{V} and a nilpotent matrix, $\mathbf{N} = \mathbf{W} - \mathbf{V} \cdot \text{diag}[\lambda_j] \cdot \mathbf{V}^{-1}$, of order r (i.e., $\mathbf{N}^r = \mathbf{0}$) for $r \leq M$ as³⁴

$$\mathbf{p}(t) = \mathbf{V} \text{diag}[e^{\lambda_j t}] \mathbf{V}^{-1} \left[\mathbf{I} + \mathbf{N}t + \dots + \frac{\mathbf{N}^{r-1} t^{r-1}}{(r-1)!} \right] \mathbf{p}(0). \quad (3.12)$$

From these solutions it is clear that in principle the conditional probability can have a multiexponential time dependence. As we see below, OCFs calculated from both KMC and MFME exhibit biexponential decay, and the MFME algebraic results produce two predominant eigen-decay rates. However, in contrast to previous studies on orientational randomization in zeolites,^{6,9} these two decay rates do *not* partition neatly into intracage motion and cage-to-cage migration.

C. Mean field theory for short times

For short times, the initial OCF decay can be characterized at any loading by a rate coefficient, $k_{\text{hop}}(\theta)$, which determines the average hop rate of a molecule at that loading. In this section we describe how this rate controls the initial OCF decay, and also derive a mean field theory (MFT) for this rate.

For short time scales the molecule either remains on its initial position or hops to a nearest-neighbor site. If we denote the probabilities for these two events as p_{on} and p_{off} , respectively, the OCF at short times is thus

$$C(t) = p_{\text{on}} P_2(\cos \gamma_{\text{on}}) + p_{\text{off}} P_2(\cos \gamma_{\text{off}}), \quad (3.13)$$

where, $\cos \gamma_{\text{on}} = 1$ and $\cos \gamma_{\text{off}} = -\frac{1}{3}$ because of the tetrahedral arrangement of nearest-neighbor sites. Using the normalization condition, $p_{\text{on}} + p_{\text{off}} = 1$, Eq. (3.13) becomes

$$C(t) = 1 - \frac{4}{3} p_{\text{off}}. \quad (3.14)$$

For short times $p_{\text{off}} \cong k_{\text{hop}}(\theta)t$ and hence $C(t) \cong 1 - \frac{4}{3} k_{\text{hop}}(\theta)t$. This expression was derived by Auerbach and Metiu⁶ for benzene in Na-Y at infinite dilution; as we show later, this expression is also valid for short times at finite loadings.

We now briefly describe the MFT for evaluating $k_{\text{hop}}(\theta)$, which depends on the population of initial sites, the jump rate coefficients from the initial to target sites, and the occupancies of target sites. As discussed above in Sec. III B 1, the probabilities P_{W} and $P_{\text{S}_{\text{II}}}$ determine the fraction of molecules starting from W and S_{II} sites, respectively, and the rate coefficients k_{11} , k_{12} , k_{21} and k_{22} (see Sec. II) determine the jump rates. θ_1 and θ_2 determine the occupancies at the W and S_{II} sites. A MFT expression incorporating these quantities is given by

$$k_{\text{hop}} = 6P_{\text{W}}[k_{11}(1 - \theta_1) + k_{12}(1 - \theta_2)] + 3P_{\text{S}_{\text{II}}}[k_{22}(1 - \theta_2) + k_{21}(1 - \theta_1)], \quad (3.15)$$

where 6 and 3 count the number of nearest-neighbors for W and S_{II} sites, respectively. We compare the results of this short-time rate to KMC and MFME data in the following section.

IV. RESULTS AND DISCUSSION

We describe the results of the study in three sections. In Sec. IV A we discuss the decay of the OCF at infinite dilution. In Sec. IV B we compare OCFs calculated with KMC and MFME methods, obtained at finite loadings in the *absence* of attractive guest-guest interactions. We also use the MFT approach to calculate short-time OCF decay rates for comparison with KMC and MFME data. Finally, in Sec. IV C we compare OCF results from MFME, MFT and KMC at finite loadings in the presence of attractive interactions.

A. Infinite dilution

For benzene in Na-Y, S_{II} sites are very stable compared to W sites (see Table I). As a result, S_{II} sites are preferentially occupied at low loadings. For example, at infinite dilution and 300 K, the fraction of molecules in the W site, P_{W} , evaluated as discussed in Sec. III B 1, is approximately 10^{-5} and hence $P_{\text{S}_{\text{II}}} \cong 1$. This implies that the first term in Eq. (3.2) can be ignored. By setting the initial condition $p(k, 0 | l = M_1 + 1, 0) = \delta_{k, M_1 + 1}$ for all k we have made it possible for the conditional probabilities, $p(k, t | M_1 + 1, 0)$, to remain approximately near their equilibrium values for all t , i.e., $p(k, t | M_1 + 1, 0) = P_{\text{S}_{\text{II}}}/32 \cong 1/32$ for $k > M_1$ and $p(k, t | M_1 + 1, 0) = P_{\text{W}}/16 \cong 0$ for $k \leq M_1$. Thus the problem of solving an $M \times M$ matrix equation is reduced to that of solving an $M_2 \times M_2$ matrix equation only involving dynamics on the S_{II} sites. However, since the S_{II} sites in a particular cage are independent from S_{II} sites in other cages, we can

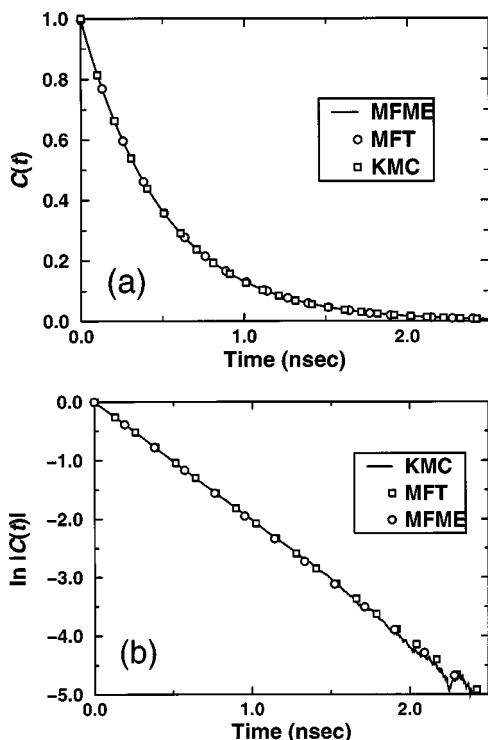


FIG. 3. (a) $C(t)$ and (b) $\ln|C(t)|$ calculated from MFME, MFT and KMC at infinite dilution and 300 K. $\ln|C(t)|$ shows simple exponential decay of OCF.

arrange these M_2 sites into $8\mathcal{N}$ sets of four nearest-neighbor S_{II} sites. This results in block diagonalizing the $M_2 \times M_2$ matrix into $8\mathcal{N}$ 4×4 identical matrices. Each of the eight identical matrix equations has the following form:

$$\begin{pmatrix} \dot{p}_1 \\ \dot{p}_2 \\ \dot{p}_3 \\ \dot{p}_4 \end{pmatrix} = \begin{pmatrix} -3k_{22} & k_{22} & k_{22} & k_{22} \\ k_{22} & -3k_{22} & k_{22} & k_{22} \\ k_{22} & k_{22} & -3k_{22} & k_{22} \\ k_{22} & k_{22} & k_{22} & -3k_{22} \end{pmatrix} \begin{pmatrix} p_1 \\ p_2 \\ p_3 \\ p_4 \end{pmatrix}, \quad (4.1)$$

where $\dot{p}_j = dp_j/dt$ for $j=1, \dots, 4$. As described in Sec. II, we have used k_{22} to denote the infinite dilution rate coefficient for the $S_{II} \rightarrow S_{II}$ hop. By determining the solution of this matrix equation in terms of the matrix eigenvalues and eigenvectors, we find very good agreement between the theory and simulation as shown in Fig. 3. The system of equations has one zero eigenvalue arising from the microscopic reversibility condition, and three identical eigenvalues, $-4k_{22}$, corresponding to the OCF decay rate. This result is consistent with a four jump site model as derived analytically by Wittebort and Szabo,³² and as simulated by Auerbach and Metiu.⁶ We can also determine the initial OCF decay rate from MFT using the same approximations employed by the MFME approach. For benzene in Na-Y at infinite dilution we have $\theta_1 \cong 0$, $\theta_2 \cong 1/M_2$, $P_W \cong 0$ and $P_{S_{II}} \cong 1$. Substituting these values into Eq. (3.15) gives the same result as MFME and KMC, i.e., $dC(t)/dt \cong -\frac{4}{3}k_{\text{hop}} = -4k_{22}$. For longer times, this short time approximation can be reexponentiated because we find single exponential OCF decay at infinite dilution using KMC and MFME, as shown in Fig. 3.

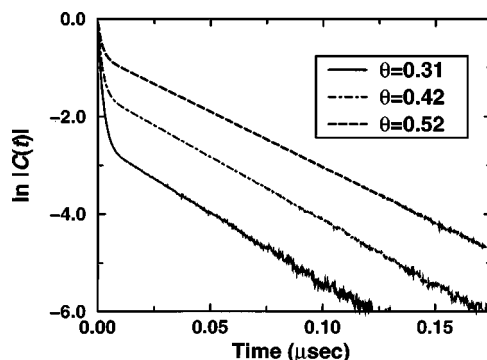


FIG. 4. Logarithm of OCFs at 300 K for $\theta=0.31, 0.42$ and 0.52 from KMC simulations, showing biexponential decay.

B. Loading (θ) dependence of OCF for $J=0$

From our MFME formulation of orientational dynamics, it is clear that OCF decay at finite loadings can, in principle, exhibit multiexponential character. However, we find that for benzene in Na-Y the OCFs can be approximated as biexponentials for all finite loadings studied. For example, Fig. 4 depicts semilog plots of OCFs evaluated at $\theta=0.31, 0.42$ and 0.52 , showing the validity of fitting these OCFs to biexponentials. From these OCFs, we extract a fast initial decay rate, k_{init} , and a slow final decay rate, k_{fin} , as a function of loading and temperature.

The MFT approach was also used to calculate the short-time decay rates for benzene in Na-Y as a function of loading. A comparison of the loading dependence of k_{init} at 300 K and 500 K from these three methods is shown in Fig. 5. We find excellent quantitative agreement among the three approaches, which is consistent with our previous finding that MFT is very accurate for times so short that at most one hop is attempted.³⁵ At 300 K and for $\theta < 0.6$, P_W and θ_1 are very small as a consequence of the energetic stability of S_{II} sites. Under these conditions and according to Eq. (3.15), k_{init} decreases linearly with respect to $\theta \cong \frac{2}{3}\theta_2$, suggesting that the equilibrium distribution of molecules for $\theta < 0.6$ only allows $S_{II} \rightarrow S_{II}$ jumps at short times. On the other hand, for $\theta > 0.6$, S_{II} sites are already filled and W sites start to be populated. All the fundamental rate constants that depend on

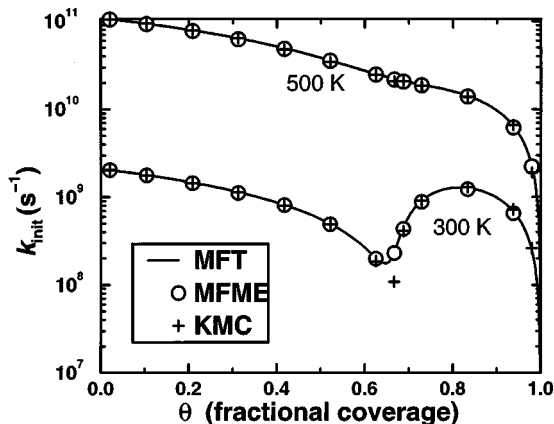


FIG. 5. k_{init} as a function of loading from KMC, MFME and MFT methods at 300 K and 500 K, without guest-guest attractions ($J=0$).

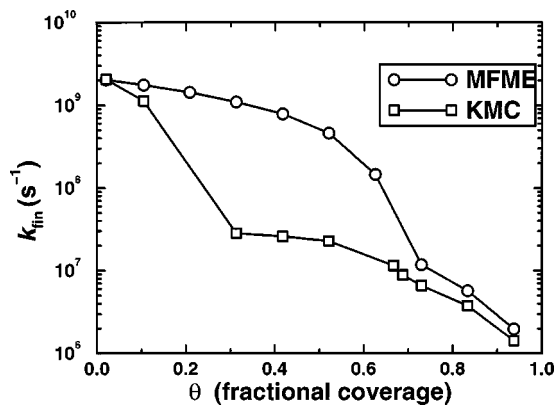


FIG. 6. k_{fin} as a function of loading from KMC and MFME methods, at 300 K and $J=0$.

θ_2 cancel out, producing a k_{init} driven by $W \rightarrow W$ and $S_{\text{II}} \rightarrow W$ transitions. The competition at high loadings between the growing P_W and the decreasing $(1 - \theta_2)$ is responsible for the parabolic shape of k_{init} at 300 K. At 500 K, W sites are more populated and k_{init} shows a smooth decay as a function of loading as appears in Fig. 5.

In general, our MFT fails to predict OCF decay for long times. Therefore we compare the results of the long-time rate constants, k_{fin} , from KMC and MFME methods in Fig. 6. Two interesting observations can be made. First, we find that the KMC rate constants are overestimated by the MFME calculations. We observe similar trends when comparing mean field approximations for diffusion coefficients with KMC results.^{18,36} Second, we observe that the MFME rate constants show maximum deviation from the KMC results at intermediate loadings, which can be understood as follows. The deviations of thermodynamic²⁸ and kinetic properties¹⁸ from mean field predictions are small at both low and high loadings, where an adsorbate is likely to experience a uniform environment of either completely empty or completely filled nearest-neighbor sites, respectively. At intermediate loadings, where density fluctuations are the largest, mean field approximations perform the worst.

We determined the temperature dependence of k_{fin} by calculating apparent activation energies, E_{app} , as a function of loading for benzene in Na-Y as shown in Fig. 7. Over the

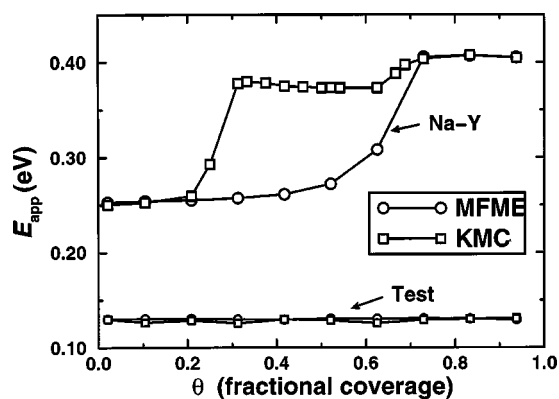


FIG. 7. Apparent activation energies, E_{app} , of k_{fin} for Na-Y and the “Test” system (see text) calculated from KMC and MFME methods.

temperature range 200–700 K, we find that k_{fin} exhibits Arrhenius temperature dependence for all loadings studied. As before, we observe that values of E_{app} obtained from MFME calculations give excellent agreement with KMC results at low and high loadings, and show maximum deviations in the intermediate loadings. Before analyzing the loading dependence of E_{app} , we discuss a test we performed to ensure that the deviations between KMC and MFME shown in Fig. 7 are real, and not the result of a programming error. We explored the origin of these deviations by testing our calculations on a model system with a single site type, a single jump rate with $E_a=0.13$ eV, and the same site topology as Na-Y. The results of these test calculations are shown in Fig. 7 labeled by “Test.” We find excellent quantitative agreement between KMC and MFME for E_{app} for all loadings, indicating that deviations between these two methods arise from energetic heterogeneities in our lattice model.

Focusing now on the “non-Test” KMC results in Fig. 7, we see that at low loadings the apparent activation energy is close to $E_a(S_{\text{II}} \rightarrow S_{\text{II}}) = 0.25$ eV. This implies that at low loadings, benzene orientational randomization is achieved primarily through intracage, $S_{\text{II}} \rightarrow S_{\text{II}}$ jumps. At intermediate loadings, i.e., $\theta \in [0.25, 0.6]$, the apparent activation energy jumps to the value of $E_a(S_{\text{II}} \rightarrow W) = 0.38$ eV, indicating that when enough S_{II} sites become occupied, full orientational randomization is achieved by making cage-to-cage jumps allowing access to vacant S_{II} sites with different orientations. The MFME apparent activation energies do not make this jump, showing that the MFME allows for intracage randomization even when KMC requires cage-to-cage motion. This is an inherent limitation of the MFME.

At high loadings $\theta \geq 0.7$, we see from Fig. 7 that the KMC-calculated apparent activation energy makes yet another jump to $E_{\text{app}}=0.4$ eV. This effect is intriguing because $E_a(S_{\text{II}} \rightarrow W) = 0.38$ eV is the largest fundamental activation energy in our model, prompting us to ask what collection of fundamental energies produces $E_{\text{app}}=0.4$ eV? We can answer this by analyzing the MFME results at high loadings, since we know that KMC and MFME energetics must and do agree in the limits of low and high loadings. In particular, the final slope of $\ln C(t)$ is controlled by the least negative, non-zero eigenvalue of the \mathbf{W} matrix in Eq. (3.9). Therefore, the dependence of k_{fin} on the fundamental kinetic parameters can be obtained by analytically diagonalizing the \mathbf{W} matrix. Unfortunately, in general the eigenvalues of \mathbf{W} are extremely complicated functions of the fundamental rate parameters, and as such yield limited conceptual information. This complexity can be avoided by considering limiting cases to simplify the analytical solution of the $M \times M$ matrix. The simplest case is the infinite dilution limit, described above, where we assumed that the molecule makes only $S_{\text{II}} \rightarrow S_{\text{II}}$ jumps. With this approximation we find an eigenvalue for the MFME of $[-4k_{22}]$, which agrees perfectly with MFT and KMC results.

For intermediate to high loadings, we simplify the MFME by assuming that molecules make only $S_{\text{II}} \rightarrow S_{\text{II}}$ and $S_{\text{II}} \rightarrow W$ jumps. Although such a system cannot obey detailed balance, the jump we have ignored for simplicity ($W \rightarrow S_{\text{II}}$) only influences short-time dynamics and as such is uninter-

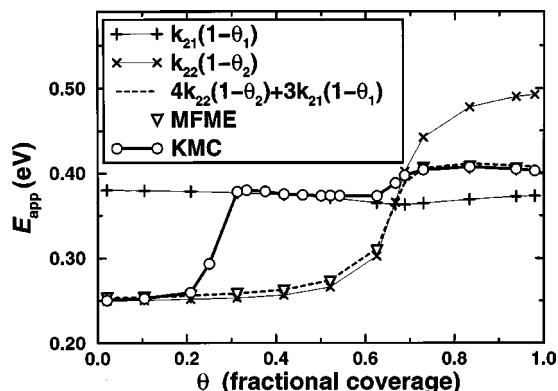


FIG. 8. Apparent activation energies, E_{app} , from k_{fin} and from fundamental rate parameters for benzene in Na-Y, calculated using KMC and MFME methods.

esting for the present discussion. The $M \times M$ matrix was reduced to an $M_2 \times M_2$ matrix in accordance with the argument described in the previous section for an infinite dilution system. Once again, we arranged this $M_2 \times M_2$ matrix into $8\mathcal{N}$ sets of 4×4 identical matrices as appear in Eq. (4.1). The off-diagonal elements of \mathbf{W} are all $k_{22}(1-\theta_2)$, where k_{22} is the infinite dilution rate coefficient and θ_2 is the equilibrium S_{II} site fractional occupancy. The diagonal terms in \mathbf{W} arise from all the possible jumps that deplete population at each S_{II} site, i.e., $-3k_{22}(1-\theta_2) - 3k_{21}(1-\theta_1)$, where k_{22} and k_{21} are the infinite dilution rates and θ_1 and θ_2 are the fractional occupancies for W and S_{II} sites, respectively. The analytical solution of this 4×4 matrix produces one nondegenerate eigenvalue $[3k_{21}(1-\theta_1)]$, and one three-fold degenerate eigenvalue $[4k_{22}(1-\theta_2) + 3k_{21}(1-\theta_1)]$. We extracted the apparent activation energies from $k_{21}(1-\theta_1)$, $k_{22}(1-\theta_2)$ and $[4k_{22}(1-\theta_2) + 3k_{21}(1-\theta_1)]$ over the range 200–700 K, and compared these to the KMC and complete-MFME activation energies shown in Fig. 8. For $\theta > 0.7$, we find excellent quantitative agreement between the activation energies from KMC and those from the analytical eigenvalue expression $[4k_{22}(1-\theta_2) + 3k_{21}(1-\theta_1)]$. This agreement strongly suggests that the apparent activation energy seen at high loadings, $E_{\text{app}} = 0.4$ eV, represents a complicated composite of fundamental intracage and intercage energetics, summarized by the formula $[4k_{22}(1-\theta_2) + 3k_{21}(1-\theta_1)]$.

C. Orientational randomization with guest-guest attractions

In the previous section we explored how site blocking can influence the loading dependence of orientational randomization rates in zeolites. Now we study the effects from both site blocking and attractive guest-guest interactions. As discussed earlier in Sec. II, we set the guest-guest lattice gas interaction parameters to $J = -0.04$ eV, obtained from the isosteric heat of adsorption.^{25,26} We have used this model to explore the loading dependence of benzene diffusion in Na-X and Na-Y,¹⁸ finding good agreement with pulsed field gradient NMR data for benzene in Na-X.²³

Despite this new level of complexity in our model, we have found that the resulting OCFs can still be well-

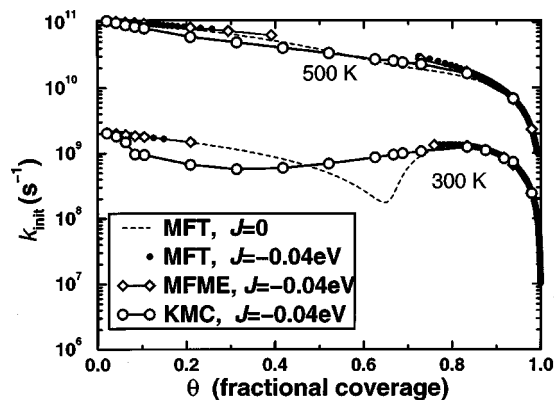


FIG. 9. Initial rates, k_{init} , as a function of loading from MFT, MFME and KMC at 300 K and 500 K, with guest-guest attractions ($J = -0.04$ eV) compared to site-blocking ($J = 0$). Mean field methods incorrectly predict coexistence regions for benzene in Na-Y (see text), shown by gaps in $J = -0.04$ eV results.

approximated as biexponential functions of time. We calculated the initial rates versus loading at 300 K and 500 K using MFT, MFME and KMC; these are shown in Fig. 9 alongside the results for $J = 0$. In contrast to the $J = 0$ results, we do not find quantitative agreement between KMC and mean field estimates of k_{init} . As expected, all these methods agree for the lowest and highest loadings, but the agreement deteriorates at intermediate loadings. The mean field methods actually predict a phase transition from low to high density of adsorbed benzene, as shown by the gaps in the mean field results that appear in Fig. 9. Although we have previously discussed such a phase transition for benzene in Na-X based on extensive grand canonical MC calculations,^{37,38} we believe that no such transition exists for benzene in Na-Y, because the Na-Y window site is too unstable to support the formation of macroscopic benzene clusters.³⁸ As such, the coexistence regions predicted in Fig. 9 are simply artifacts of mean field methods.

The long-time decay rate, k_{fin} , is plotted in Fig. 10 as a function of loading for $T = 300$ K. This shows the now-familiar pattern of agreement between KMC and MFME at low and high loadings, with MFME overestimating KMC decay rates at intermediate loadings. The marked difference

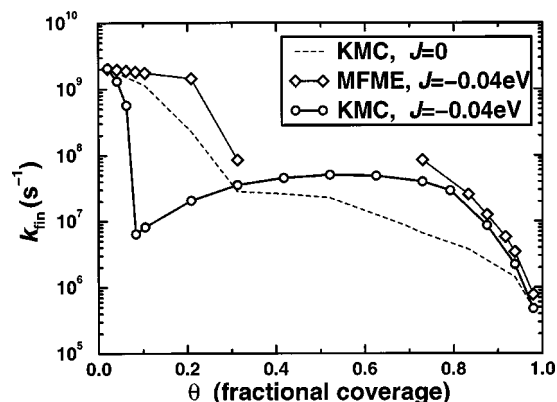


FIG. 10. k_{fin} as a function of loading at 300 K from MFME and KMC, comparing results for $J = 0$ and -0.04 eV. As with k_{init} , MFME incorrectly predicts a coexistence region.

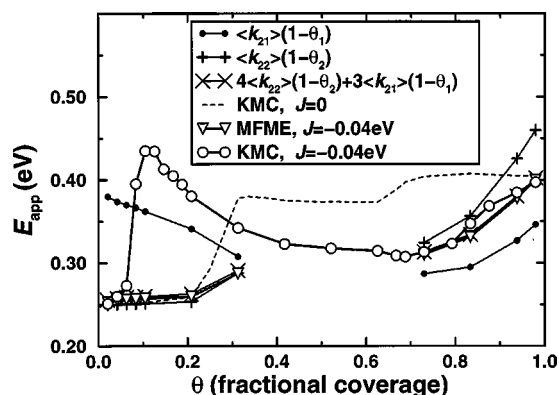


FIG. 11. Apparent activation energies, E_{app} , from k_{fin} and from fundamental rate parameters as a function of loading using KMC and MFME methods. The artifactual mean field coexistence region precludes showing points in the range $\theta \in (0.32, 0.72)$.

between the two KMC curves shows the result of including attractive guest-guest attractions, which we discuss further later.¹⁸

We now explore the apparent activation energy associated with benzene orientational randomization in the presence of guest-guest attractions. These activation energies are plotted in Fig. 11 alongside the $J=0$ KMC results, as well as the apparent activation energies from various fundamental rate parameters. In particular, we plot the apparent activation energy of $\langle k_{2 \rightarrow j} \rangle (1 - \theta_j)$, where $\langle k_{2 \rightarrow j} \rangle$ is the mean field average of $k_{2 \rightarrow j}$ and θ_j is the mean field fractional coverage of site type $j=1,2$, all with guest-guest attractions according to the parabolic jump model.¹⁸ We also plot the E_{app} associated with $[4 \langle k_{22} \rangle (1 - \theta_2) + 3 \langle k_{21} \rangle (1 - \theta_1)]$, since this eigenvalue of the \mathbf{W} matrix controls the long-time OCF decay as shown above. Once again we see in Fig. 11 that MFME agrees with KMC at the lowest and highest loadings, but MFME fails to describe the KMC results even qualitatively, especially at loadings below $\theta=0.6$. It is interesting that while the temperature dependence of MFME quantitatively follows that of $[4 \langle k_{22} \rangle (1 - \theta_2) + 3 \langle k_{21} \rangle (1 - \theta_1)]$, the temperature dependence of the KMC results qualitatively follows that of $\langle k_{21} \rangle (1 - \theta_1)$ above loadings of $\theta=0.1$. The same mirroring effect of KMC results by $k_{21}(1 - \theta_1)$ is not seen for $J=0$ in Fig. 8.

Perhaps the most striking finding in Fig. 11 is the effect on KMC activation energies from including guest-guest attractions. Indeed, while the $J=0$ KMC activation energies are roughly constant up to $\theta=0.2$, those arising from guest-guest attractions show a rapid rise and fall in the same loading regime. Moreover, while the $J=0$ activation energies remain constant at 0.4 eV for loadings above $\theta=0.7$, those arising from guest-guest attractions exhibit a monotonic increase from 0.3 to 0.4 eV in this loading regime.

Focusing now on the loading of five molecules per cage ($\theta=0.83$) for comparison with the NMR data of Isfort *et al.*,¹³ we find $E_{app}=0.4$ eV in the absence of guest-guest attractions, and 0.34 eV in the presence of such attractions. We find it interesting that $E_{app}(J=0) > E_a(S_{II} \rightarrow W)$ while $E_{app}(J < 0) < E_a(S_{II} \rightarrow W)$, where $E_a(S_{II} \rightarrow W)$ is the fundamental activation energy for $S_{II} \rightarrow W$ jumps. As such, includ-

ing guest-guest attractions produces qualitative changes in the way we compare our results with experiment. In particular, the NMR data of Isfort *et al.*¹³ yield an $E_{app}=40$ kJ mol⁻¹=0.41 eV, which agrees well with our site blocking result, and is 0.07 eV greater than the result from our model with guest-guest attractions. This, of course, does *not* suggest that our site blocking model is more accurate; indeed, the agreement seen between the NMR data and the site blocking model is surely fortuitous cancellation of many errors. This result does suggest, however, that the actual $S_{II} \rightarrow W$ barrier is greater than 40 kJ mol⁻¹, since in our best KMC simulations we find that $E_a(S_{II} \rightarrow W) > E_{app}(J < 0)$. Several atomistic simulations of the $S_{II} \rightarrow W$ barrier for benzene in Na-Y yield results in the range of 41–49 kJ mol⁻¹,^{14–16} which agrees well with our interpretation of the NMR data.

Applying this same kind of analysis to diffusion data also works well. In particular, we have shown that E_{app} for benzene diffusion in Na-Y at infinite dilution is given by $E_a(S_{II} \rightarrow W)$,³⁹ which we have taken to be 0.38 eV in this and in previous studies.¹⁸ However, at the loading $\theta=0.21=1.3/6$ molecules per cage, we found $E_{app}=31.2$ kJ mol⁻¹=0.324 eV for benzene self-diffusion in Na-Y, reported in Ref. 18. Moreover, recent quasi-elastic neutron scattering (QENS) measurements find $E_{app}=33.7$ kJ mol⁻¹ for two molecules of benzene in each Na-Y cage. Our KMC results thus suggest that the fundamental $S_{II} \rightarrow W$ barrier is well above the QENS apparent activation energy, lending further credence to the atomistic simulations already carried out on benzene in Na-Y.^{14–16}

V. CONCLUDING REMARKS

We have developed a lattice model to study the orientational dynamics of benzene in Na-Y zeolite, motivated by the recent two-dimensional exchange NMR study of Isfort *et al.* on this system at benzene loadings near five molecules per cage.¹³ The goal of our study is to determine how the interplay between host-guest and guest-guest interactions influences the time and temperature dependencies of benzene orientational randomization in Na-Y. We consider guest-guest interactions in two stages. First we include only site-blocking interactions; next we consider both site blocking and nearest-neighbor attractive interactions.

We calculated orientational correlation functions (OCFs) using kinetic Monte Carlo (KMC) simulations, and also approximately using a mean field master equation (MFME). Both methods produce OCFs exhibiting biexponential decay in time. We also developed an analytical mean field theory for the initial decay rate, which is exact for the site-blocking model but only approximate when attractive guest-guest interactions are considered. We then solved the site-blocking MFME numerically and analytically for the activation energy associated with the long-time decay rate, for comparison with KMC results. The MFME activation energies agree very well with KMC results at low and high loadings, but consistently underestimate KMC activation energies at intermediate loadings. At finite loadings the MFME allows intracage randomization, while KMC requires cage-to-cage motion for complete randomization. At high loadings, where the

MFME is accurate, its analytical solution shows that the long-time decay is controlled by a composite of $S_{II} \rightarrow S_{II}$ and $S_{II} \rightarrow W$ jump processes.

We have found that at high loadings, the apparent activation energy for long-time OCF decay satisfies $E_{app}(J=0) > E_a(S_{II} \rightarrow W)$ while $E_{app}(J<0) < E_a(S_{II} \rightarrow W)$, where $E_a(S_{II} \rightarrow W)$ is the fundamental activation energy for $S_{II} \rightarrow W$ jumps, and $J < 0$ controls the strength of guest-guest attractions. This shows the qualitative importance of including guest-guest attractions in such models, and also suggests that the actual $S_{II} \rightarrow W$ barrier is greater than the 40 kJ mol⁻¹ apparent activation energy measured by Isfort *et al.*¹³ This conclusion lends credence to atomistic simulations of the $S_{II} \rightarrow W$ barrier for benzene in Na–Y, which yield results in the range of 41–49 kJ mol⁻¹.^{14–16}

In future work, we plan to explore the influences of fluid phase transitions on molecular orientational randomization in zeolites. We have previously simulated benzene adsorption in Na–X and Na–Y zeolites using the lattice model described above.^{37,38} For Na–X, critical temperatures as high as 300–400 K are found for reasonable values of the parameters, while for Na–Y no phase transition is predicted. The phase transition for benzene in Na–X arises because of strong attractions between benzene molecules in adjacent cages. These interactions are mediated by benzene molecules in W sites, which are shared between adjacent supercages, thereby stabilizing large clusters of coupled benzenes. For benzene in Na–Y, our simulations predict that the Na–Y W site is too unstable to support the development of such large clusters. We have explored the influence of this phase transition on benzene diffusion in Na–X,¹⁸ finding qualitatively different loading dependencies in subcritical and supercritical regimes. However, it is not obvious how such a phase transition might influence orientational randomization of molecules in zeolites. The development of such models is complicated by the difficulty of experimentally locating benzene in Na–X near W sites.⁴⁰

ACKNOWLEDGMENTS

This work was supported by the National Science Foundation (CHE-9616019 and CTS-9734153), a Sloan Foundation Research Fellowship (BR-3844), and a Camille Dreyfus Teacher-Scholar Award (TO-99-041).

¹J. Kärger and D. M. Ruthven, *Diffusion in Zeolites and Other Microporous Solids* (Wiley, New York, 1992).

²N. Y. Chen, T. F. Degnan, Jr., and C. M. Smith, *Molecular Transport and Reaction in Zeolites* (VCH, New York, 1994).

³P. Demontis and G. B. Suffritti, *Chem. Rev.* **97**, 2845 (1997).

⁴S. M. Auerbach, *Int. Rev. Phys. Chem.* **19**, 155 (2000).

⁵S. M. Auerbach and F. Jousse, "Dynamics of sorbed molecules in zeo-

lites," in *Computer Modelling of Microporous and Mesoporous Materials*, edited by C. R. A. Catlow, R. A. van Santen, and B. Smit (Academic, London, submitted).

⁶S. M. Auerbach and H. I. Metiu, *J. Chem. Phys.* **106**, 2893 (1997).

⁷B. Boddenberg and B. Beerwerth, *J. Phys. Chem.* **93**, 1440 (1989).

⁸L. M. Bull, N. J. Henson, A. K. Cheetham, J. M. Newsam, and S. J. Heyes, *J. Phys. Chem.* **97**, 11776 (1993).

⁹J. A. Sousa-Gonçalves, R. L. Portsmouth, P. Alexander, and L. F. Gladden, *J. Phys. Chem.* **99**, 3317 (1995).

¹⁰D. E. Favre, D. J. Schaefer, and B. F. Chmelka, *J. Magn. Reson.* **134**, 261 (1998).

¹¹D. E. Favre, D. J. Schaefer, S. M. Auerbach, and B. F. Chmelka, *Phys. Rev. Lett.* **81**, 5852 (1998).

¹²D. J. Schaefer, D. E. Favre, M. Wilhelm, S. J. Weigel, and B. F. Chmelka, *J. Am. Chem. Soc.* **119**, 9252 (1997).

¹³O. Isfort, B. Boddenberg, F. Fujara, and R. Grosse, *Chem. Phys. Lett.* **288**, 71 (1998).

¹⁴S. M. Auerbach, N. J. Henson, A. K. Cheetham, and H. I. Metiu, *J. Phys. Chem.* **99**, 10600 (1995).

¹⁵F. Jousse and S. M. Auerbach, *J. Chem. Phys.* **107**, 9629 (1997).

¹⁶T. Mosell, G. Schrimpf, and J. Brickmann, *J. Phys. Chem. B* **101**, 9476 (1997).

¹⁷C. Saravanan, F. Jousse, and S. M. Auerbach, *Phys. Rev. Lett.* **80**, 5754 (1998).

¹⁸C. Saravanan and S. M. Auerbach, *J. Chem. Phys.* **110**, 11000 (1999).

¹⁹R. L. June, A. T. Bell, and D. N. Theodorou, *J. Phys. Chem.* **95**, 8866 (1991).

²⁰A. N. Fitch, H. Jovic, and A. Renouprez, *J. Phys. Chem.* **90**, 1311 (1986).

²¹P. H. Nelson and S. M. Auerbach, *Chem. Eng. J.* **74**, 43 (1999).

²²M. C. Mitchell, A. V. McCormick, and H. T. Davis, *Z. Phys. B: Condens. Matter* **97**, 353 (1995).

²³A. Germanus, J. Kärger, H. Pfeifer, N. N. Samulevic, and S. P. Zdanov, *Zeolites* **5**, 91 (1985).

²⁴E. S. Hood, B. H. Toby, and W. H. Weinberg, *Phys. Rev. Lett.* **55**, 2437 (1985).

²⁵D. Barthomeuf and B. H. Ha, *J. Chem. Soc., Faraday Trans.* **69**, 2147 (1973).

²⁶D. Barthomeuf and B. H. Ha, *J. Chem. Soc., Faraday Trans.* **69**, 2158 (1973).

²⁷P. Maksym, *Semicond. Sci. Technol.* **3**, 594 (1988).

²⁸D. Chandler, *Introduction to Modern Statistical Mechanics* (Oxford University Press, New York, 1987).

²⁹W. H. Press, S. A. Teukolsky, W. T. Vetterling, and B. P. Flannery, *Numerical Recipes in Fortran* (Cambridge University Press, New York, 1992).

³⁰C. Saravanan and S. M. Auerbach, *J. Chem. Phys.* **107**, 8120 (1997).

³¹N. G. van Kampen, *Stochastic Processes in Physics and Chemistry* (North Holland, New York, 1981).

³²R. J. Wittebort and A. Szabo, *J. Chem. Phys.* **69**, 1722 (1978).

³³I. Oppenheim, K. E. Shuler, and G. H. Weiss, *Stochastic Processes in Chemical Physics: The Master Equation* (MIT, Cambridge, MA, 1977).

³⁴L. Perko, *Differential Equations and Dynamical Systems* (Springer-Verlag, New York, 1993).

³⁵P. H. Nelson and S. M. Auerbach, *J. Chem. Phys.* **110**, 9235 (1999).

³⁶C. Saravanan, F. Jousse, and S. M. Auerbach, *J. Chem. Phys.* **108**, 2162 (1998).

³⁷C. Saravanan and S. M. Auerbach, *J. Chem. Phys.* **109**, 8755 (1998).

³⁸I. Dukovski, J. Machta, C. Saravanan, and S. M. Auerbach, *J. Chem. Phys.* **113**, 3697 (2000).

³⁹S. M. Auerbach, *J. Chem. Phys.* **106**, 7810 (1997).

⁴⁰G. Vitale, C. F. Mellot, L. M. Bull, and A. K. Cheetham, *J. Phys. Chem. B* **101**, 4559 (1997).